Hindawi
Mathematical Problems in Engineering
Volume 2018, Article ID 3268962, 16 pages
https://doi.org/10.1155/2018/3268962

Research Article

Rehabilitation Effect Evaluation of CFRP-Lined Prestressed Concrete Cylinder Pipe under Combined Loads Using Numerical Simulation

He Hu,[1,2] **Fujun Niu**,[1,2] **Tiesheng Dou**,[3] **and Heng Zhang**[1,2]

[1]*South China Institution of Geotechnical Engineering, School of Civil Engineering and Transportation, South China University of Technology, Guangzhou, China*
[2]*State Key Laboratory of Subtropical Building Science, South China University of Technology, Guangzhou, China*
[3]*China Institute of Water Resources and Hydropower Research, Beijing, China*

Correspondence should be addressed to Fujun Niu; niufujun@lzb.ac.cn

Received 31 July 2018; Revised 26 October 2018; Accepted 28 October 2018; Published 11 November 2018

Academic Editor: Jose A. Reinoso

Prestressed concrete cylinder pipe (PCCP) has been widely used for water transfer and transit projects. However, prestressing wire breaks may result in the rupture of pipes and cause catastrophes. Carbon fiber reinforced polymer (CFRP) liners adhered to the inner concrete core can provide an effective method of internal repair and strengthening of PCCP. To evaluate the rehabilitation effect of CFRP-lined PCCP under combined loads, two contrasting three-dimensional finite element models that investigated the visual cracking of concrete and the yielding of steel cylinders were developed. A conceptual zone was introduced to analyze the different states of the pipe during the phase of wire break. In particular, the complex CFRP-concrete bonded interface was simulated by a cohesive element layer with a bilinear traction-separation response. The results show that CFRP has a good rehabilitation effect on the inner concrete core and steel cylinder but only a slight effect on the outer concrete core, prestressing wire, or mortar. A one-hoop CFRP layer diminishes the area of a yielding steel cylinder of 4.72 m^2. In addition, CFRP works more effectively along with an increase in the number of broken wires. This research can provide a basis for strengthening distressed PCCP pipelines.

1. Introduction

Prestressed concrete cylinder pipe (PCCP) has been widely used in many areas including municipal, industrial, and water diversion because of its structural advantages such as a large diameter, low water head loss, and strong earthquake resistance. PCCP generally consists of a concrete core, high-tensile steel wires that spirally wound around the concrete, a steel cylinder encased in concrete, and a mortar coating layer. The prestressing wires are typically designed to withstand all of the hydrostatic pressure. Owing to corrosion and hydrogen embrittlement, prestressing wire may break. If many wires broke, the rupture of pipe can lead to a catastrophe. Therefore, it is necessary for water supply engineers to understand the wire-break process of PCCP and determine a feasible repair plan.

Combined with former theories and technologies, some methods were proposed to rehabilitate PCCP. However, all these methods require excavation of the cover soil and processing of the complicated construction technologies by heavy machinery, which are costly and time-consuming [1–4]. Installing carbon fiber reinforced polymer (CFRP) on the inner concrete to strengthen PCCP is an effective way to minimize these negative effects.

Lee and Karbhari [5] conducted an extensive test program with prefabricated FRP and wet layup of fabric-strengthened PCCP sections to verify the feasibility of this method. Zarghamee et al. [6] reported that the water tightness of CFRP liner can be improved by introducing an impervious glass layer in the CFRP laminate, painting polyurethane coating on the inside surface of the laminate, and increasing the number of CFRP layers. Gong et al. [7] conducted a

Figure 1: Typical CFRP-lined PCCP.

full-scale experiment of new-type jacking PCCP to evaluate the structural performance of pipe.

Lee et al. [8] proposed a simplifying function for the horizontal deflection of buried PCCP considering the pipe-soil interaction. Xiong et al. [9] took the contribution of the wire stiffness of PCCP into account and developed a wire-wrapping model to simulate the process of wrapping wire. Hajali et al. [10] analyzed the structural performance of PCCP with broken wires at the spigot joint, bell joint, and barrel using a numerical model.

To study the nonlinear behavior and ultimate resisting capacity of a CFRP-repaired concrete structure, many numerical modeling methods have been adopted [11–15], providing a basic understanding of the FRP-concrete interface. For PCCP, Zarghamee et al. [16] designed a bundle of composite four connector elements to simulate the bonding properties of an FRP-concrete interface in a two-dimensional model. Similarly, Lee et al. [17] used spring elements to connect CFRP liner to concrete.

Installing CFRP liner, a completely new method for PCCP renewal, has a distinctive failure pattern [18, 19] and is still under investigation. In this study, two contrasting models for PCCP and CFRP-lined PCCP were developed to evaluate the rehabilitation effect. The article focused on a CFRP-concrete interface modeled by a cohesive element layer. The main evaluation indexes of the rehabilitation effect were the visual cracking of concrete and mortar and the yielding of steel cylinder.

2. Model Geometrical Characteristics

The main function of PCCP is to divert water resources under internal loads plus external soil pressure. Therefore, maintaining a safe service state under combined loads is the essential level that the pipe must reach. For the finite element (FE) models, a three-dimensional model A of PCCP and another model B of CFRP-lined PCCP with one longitudinal CFRP and one hoop CFRP under combined loads are developed by using the ABAQUS/Standard program. Obviously, the hoop CFRP is designed to improve the hoop structural performance of distressed pipe. In the distressed pipe, bending between the broken wire zone without any prestress and the adjacent zone where it is affected by the broken wire zone will cause uneven radial displacement. This displacement may result in transverse gaps between waves of CFRP. As a result, water can bypass the CFRP liner through gaps, rendering the liner ineffective [20]. The longitudinal CFRP is designed to meet this longitudinal strain demand. To this end, CFRP laminate is the only difference between model A and model B.

2.1. PCCP Size. CFRP-lined PCCP consists of various FRP layers and PCCP components. Figure 1 illustrates a typical pipe. The size parameters of the pipe for this application are given as follows.

The internal working pressure P_w = 0.8 MPa. The geometrical parameters of PCCP were the inner diameter of the pipe D_i = 4000 mm, outer diameter of the cylinder D_y = 4183 mm, the total concrete thickness of including cylinder h_c = 350 mm, the thickness of the steel cylinder t_y = 2 mm, the wire diameter d_s = 7 mm, the wire spacing d = 14.3 mm, the thickness of coating mortar h_m = 32 mm, the length of the pipe l = 5000 mm, and the height of earth cover over pipe H = 2.8 m. After absorbing certain epoxy resin, carbon fiber waves then thicken. For CFRP, the mean thickness of each layer h_{CFRP} = 0.75 mm. A schematic and detailed drawing of CFRP-lined PCCP are shown in Figure 2. There were no CFRP and cohesive element layer in model A.

2.2. Various Backfilling Areas. To prevent the PCCP from cracking under different embankment conditions, the backfilling soil and bedding soil of the pipe can be divided into several zones. In these models, the surrounding soil of PCCP was partitioned into six different areas: the in situ soil, bedding soil zone, backfilling soil zone A, the foundation of the pipe, buffering soil zone, and backfilling soil zone B, as shown in Figure 3(a). Each zone had a particular property. According to Lotfi et al. [21], Katona [22], and Alzabeebee et al. [23], the width of the calculating model was determined to be five times the outside diameter of the pipe.

2.3. Mesh and Boundary Conditions. In these two models, every component was meshed based on the geometric characteristics. Soil, concrete, and mortar were simulated using three-dimensional eight-node brick elements (C3D8R). An eight-node three-dimensional cohesive element (COH3D8) layer was used to model the CFRP-concrete interface. According to the property of the cohesive element, CFRP could be meshed with C3D8R element. The prestressing wire was simulated using a three-dimensional truss element (T3D2). A four-node, quadrilateral, stress/displacement shell element with reduced integration (S4R) was used to represent the steel cylinder. Furthermore, the C3D8R and S4R elements adopted the total stiffness approach as the hourglass control approach. The concrete core, mortar, prestressing wires, steel cylinder, and soil had 9600,

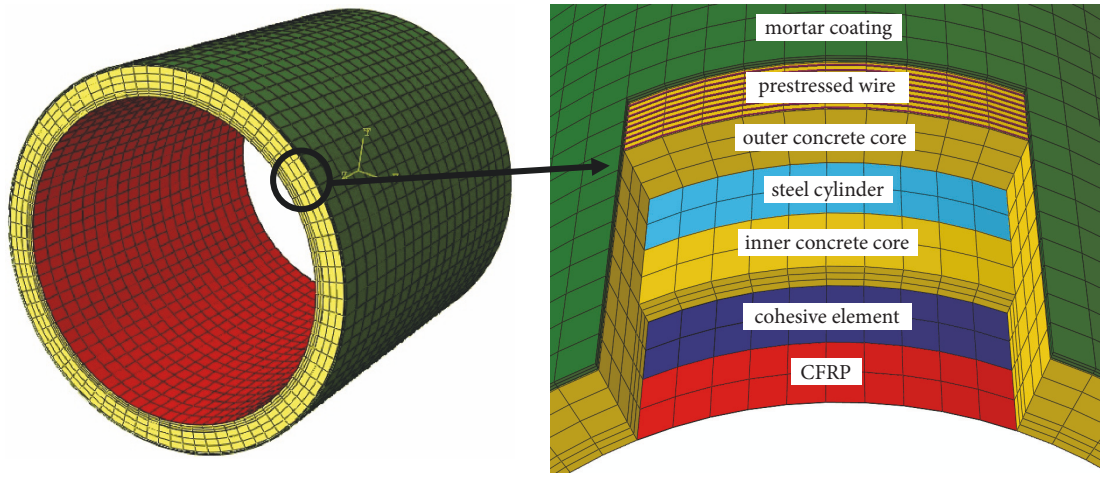

Figure 2: FE model of CFRP-lined PCCP: (a) schematic diagram and (b) detailed drawing.

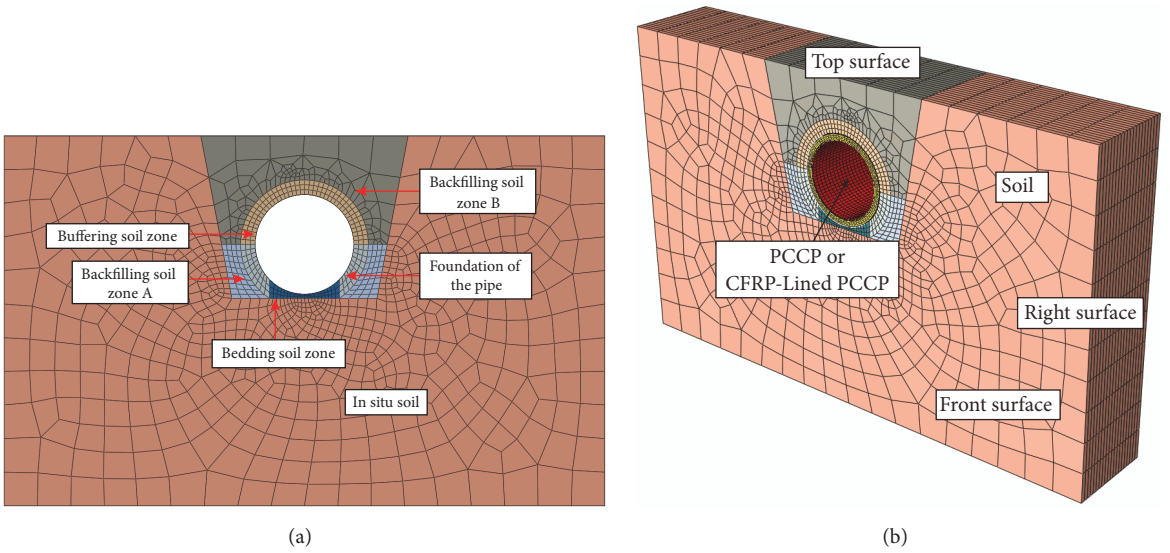

Figure 3: Soil and entire assembly of FE mesh model: (a) six different zones of surrounding soil and (b) three-dimensional mesh geometry.

4800, 28000, 1600, and 21000 elements, respectively. The cohesive element layer and CFRP had 1600 and 3200 elements, respectively. The entire model is shown in Figure 2(b).

With regard to the boundary conditions, the nodes on the bottom surface of the model were fully fixed, the nodes on the top surface of the model were free, the nodes on the left and right surfaces of the model were specified with no horizontal displacement or rotation because of the vertical consolidation settlement, and the nodes on the front and back surfaces of the model were restricted in the pipeline longitudinal direction. Typical loads such as the weight of soil, pipe, and internal/surge pressure were considered in the model.

3. Modeling Approach

3.1. Constitutive Model. Concrete and mortar are both brittle materials and have two main failure mechanisms: tensile cracking and compressive crushing. The concrete damaged plasticity (CDP) model in the ABAQUS material model can be used to present these two failure patterns by accounting for the tensile equivalent plastic strains $\tilde{\varepsilon}_t^{pl}$ and compressive equivalent plastic strains $\tilde{\varepsilon}_c^{pl}$. The evolution of the yield surface is also determined by $\tilde{\varepsilon}_t^{pl}$ and $\tilde{\varepsilon}_c^{pl}$. Typical uniaxial tensile and compressive stress-strain curves are shown in Figures 4(a) and 4(b), respectively. After reaching the failure stress σ_{t0} or ultimate stress σ_{cu}, the stress-strain curves are inclined to show a strain-softening tendency accompanied by

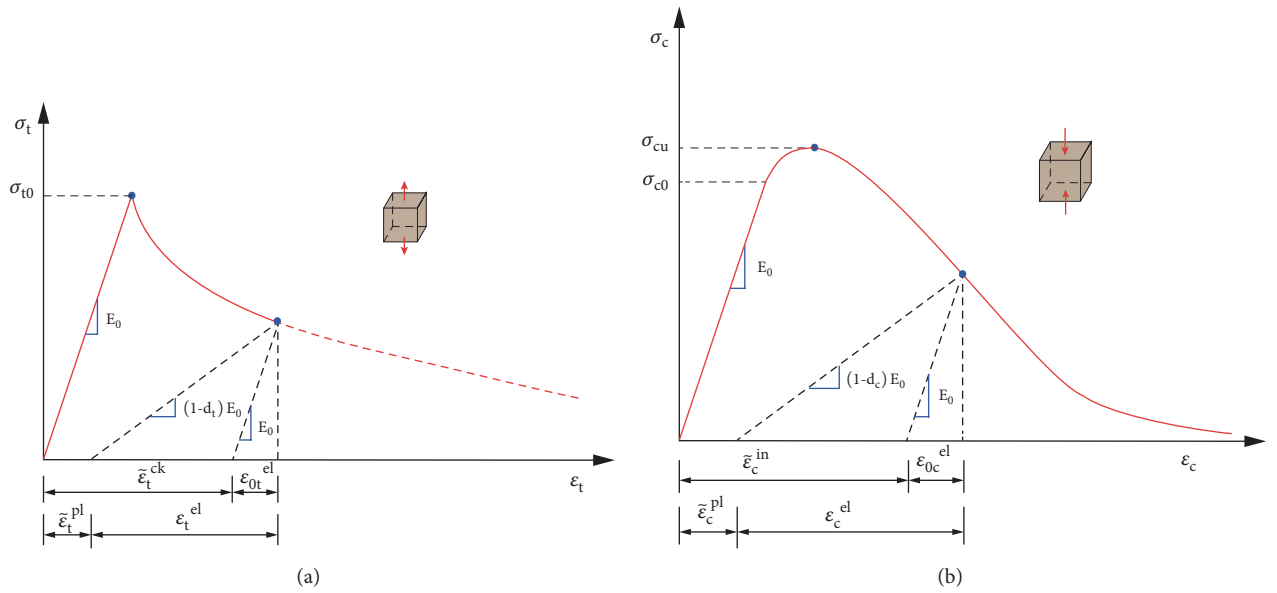

Figure 4: Concrete constitutive relationship curves: (a) concrete uniaxial tensile curve and (b) concrete uniaxial compressive curve.

elastic stiffness being damaged. Thus, two damage variables d_t and d_c are introduced to characterize the degradation of the elastic stiffness for tension and compression behavior, respectively. The strain-softening branch can be described as (1) for tension behavior and (2) for compression behavior:

$$\sigma_t = (1 - d_t) E_0 \left(\varepsilon_t - \tilde{\varepsilon}_t^{pl}\right), \tag{1}$$

$$\sigma_c = (1 - d_c) E_0 \left(\varepsilon_c - \tilde{\varepsilon}_c^{pl}\right). \tag{2}$$

σ_t and σ_c are the stress in the softening branch, and ε_t and ε_c are the strain in the softening branch. E_0 is the undamaged elastic modulus.

On the other hand, strain softening also decreases the elastic modulus. The reduction of the elastic modulus E is calculated by the following equation:

$$\mathrm{E} = (1 - d) E_0, \tag{3}$$

where d is the scalar degradation variable, which is a function of the uniaxial damage variables d_t and d_c, and $0 \le \mathrm{d} \le 1$.

$$\mathrm{d} = 1 - (1 - s_t d_c)(1 - s_c d_t). \tag{4}$$

s_t and s_c are parameters of the stiffness recovery effects associated with stress reversals [24].

In terms of the effective stresses, the yield function takes the following form [25, 26]:

$$\mathrm{F} = \frac{1}{1-\alpha}\left(\overline{q} - 3\alpha\overline{p} + \beta\left(\tilde{\varepsilon}^{pl}\right)\left\langle\hat{\overline{\sigma}}_{max}\right\rangle - \gamma\left\langle-\hat{\overline{\sigma}}_{max}\right\rangle\right) - \overline{\sigma}_c\left(\tilde{\varepsilon}_c^{pl}\right) = 0, \tag{5}$$

with

$$\alpha = \frac{(\sigma_{b0}/\sigma_{c0}) - 1}{2(\sigma_{b0}/\sigma_{c0}) - 1}; \quad 0 \le \alpha \le 0.5, \tag{6}$$

$$\beta = \frac{\overline{\sigma}_c\left(\tilde{\varepsilon}_c^{pl}\right)}{\overline{\sigma}_t\left(\tilde{\varepsilon}_t^{pl}\right)}(1 - \alpha) - (1 + \alpha), \tag{7}$$

$$\gamma = \frac{3(1 - K_c)}{2K_c - 1}. \tag{8}$$

$\overline{q}$ is the Mises equivalent effective stress; $\overline{p}$ is the hydrostatic stress; $\hat{\overline{\sigma}}_{max}$ is the maximum principal effective stress; $\langle\ \rangle$ is the Macauley bracket, which can be defined by $\langle x\rangle = (|x| + x)/2$; σ_{b0}/σ_{c0} denotes the ratio of the initial equibiaxial compressive yield stress to the initial uniaxial compressive yield stress; K_c represents the ratio of the second stress invariant on the tensile meridian q(TM) to that on the compressive meridian q(CM) at the initial yield for any given value of the pressure invariant p; $\overline{\sigma}_c(\tilde{\varepsilon}_c^{pl})$ and $\overline{\sigma}_t(\tilde{\varepsilon}_t^{pl})$ are the effective compressive and tensile cohesion stresses, respectively; and $\overline{\sigma}_c^{pl}$ and $\overline{\sigma}_t^{pl}$ are, respectively, the compressive and tensile equivalent plastic strains. The compressive stresses and strains are positive, and the tensile stresses and strains are negative. The yield surfaces in the deviatoric face with different K_c are shown in Figure 5.

The plastic flow rule determines the direction and magnitude of plastic deformation. The CDP model utilizes a nonassociated Drucker-Prager hyperbolic function to define potential function G:

$$\mathrm{G} = \sqrt{(e\sigma_{t0}\tan\psi)^2 + \overline{q}^2} - \overline{p}\tan\psi = 0. \tag{9}$$

e is the eccentricity that controls the rate at which the plastic potential function approaches the asymptote, σ_{t0} is the

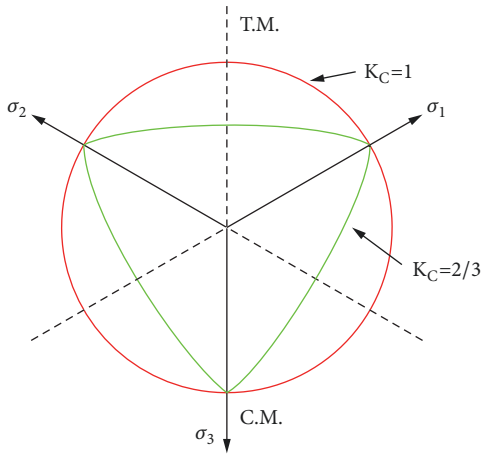

Figure 5: Yield surface in the deviatoric face with different K_c.

uniaxial tensile stress, and ψ is the dilation angle measured in the p-q plane.

The gross wrapping stress of the prestressing wire f_{sg} is 75% of the specified minimum tensile strength of the wire, as shown in (10). The yield strength of the wire f_{sy} is 85% of the specified minimum tensile strength of the wire, as shown in (11). The constitutive relationship for the prestressing wire, after wrapping at f_{sg}, can be given in (12) [27].

$$f_{sg} = 0.75 f_{su}, \tag{10}$$

$$f_{sy} = 0.85 f_{su}, \tag{11}$$

$$f_s = \varepsilon_s E_s \quad for\ \varepsilon_s \le \frac{f_{sg}}{E_s}$$

$$f_s = f_{su}\left\{1 - \left[1 - 0.6133\left(\frac{\varepsilon_s E_s}{f_{su}}\right)\right]^{2.25}\right\} \tag{12}$$

$$for\ \varepsilon_s > \frac{f_{sg}}{E_s}$$

where ε_s is the strain of the prestressing wire and f_{su} is the specified minimum tensile strength of the wire.

The steel cylinder adopts the von Mises elastoplastic stress-strain relationship with a linear elastic branch and a constant stress after reaching the yield strength.

CFRP is treated as an orthotropic elastic-brittle material. In the fiber direction, once the stress reaches the ultimate tensile strength, CFRP will fracture. The unidirectional fiber laminate thickness, each fiber orientation, and constitutive constants are required as input for the numerical model of the CFRP liner. Regarding the surrounding soils, a modified Mohr-Coulomb model is used to calculate earth loads on PCCP buried pipes.

3.2. Material Parameters. The concrete core was modeled with a compressive strength of 44.00 MPa and a tensile strength of 3.86 MPa. The mortar coating had a compressive strength and tensile strength of 47.5 MPa and 3.58 MPa, respectively. The uniaxial stress-strain relationships of the concrete and mortar were based upon a current standard [28]. The prestressing wire had an ultimate strength f_{su} of 1,570 MPa. The steel cylinder was a mild steel with a yield strength of 225 MPa. The detailed parameters of PCCP and the soil properties are listed in Table 1 [29]. The CFRP was a composite material with a high tensile strength of 600 MPa in the longitudinal direction of the fiber but a low tensile strength in the transverse direction. The material properties of CFRP are listed in Table 2.

3.3. Interaction between Components

3.3.1. Interaction inside Pipe and Pipe-Soil Interaction. All components in model A and model B were modeled as independent parts. Then, all parts were assembled together as an entire model. The interactions between components were vital to the composite pipe. The steel cylinder was embedded into the concrete core. Meanwhile, the prestressing wire was also embedded into the mortar coating. Concrete and mortar were completely tied together without considering delamination. The interface between the pipe and soil was modeled by surface-to-surface contact with small sliding, in which the value of the interface friction was 0.35. Through utilizing the temperature-drop method, the prestress was applied to the prestressing wire.

3.3.2. Cohesive Element in CFRP-Concrete Interface. The CFRP-concrete interface has complex relationships, containing ruptures, debonding, and shearing behaviors [30–32]. A cohesive element layer with a bilinear traction-separation response was introduced to simulate the bonded interface. The traction-separation model includes three components: initial linear elastic behavior, damage initiation criterion, and linear damage evolution law. A typical bilinear traction-separation model is shown in Figure 6(a).

The initial elastic behavior relates the nominal stresses to the nominal strains across the interface by an elastic constitutive matrix. The nominal stresses are the force components that present the traction variables, and the nominal strains present the separation variables. In a three-dimensional model, the nominal traction stress vector $\boldsymbol{t}$ consists of t_n, t_s, and t_t, which present the stress when the deformation is either purely normal to the interface or purely in the first or the second shear direction, respectively. The corresponding strains can be denoted by the following equation:

$$\varepsilon_n = \frac{\delta_n}{T_0},$$

$$\varepsilon_s = \frac{\delta_s}{T_0}, \tag{13}$$

$$\varepsilon_t = \frac{\delta_t}{T_0},$$

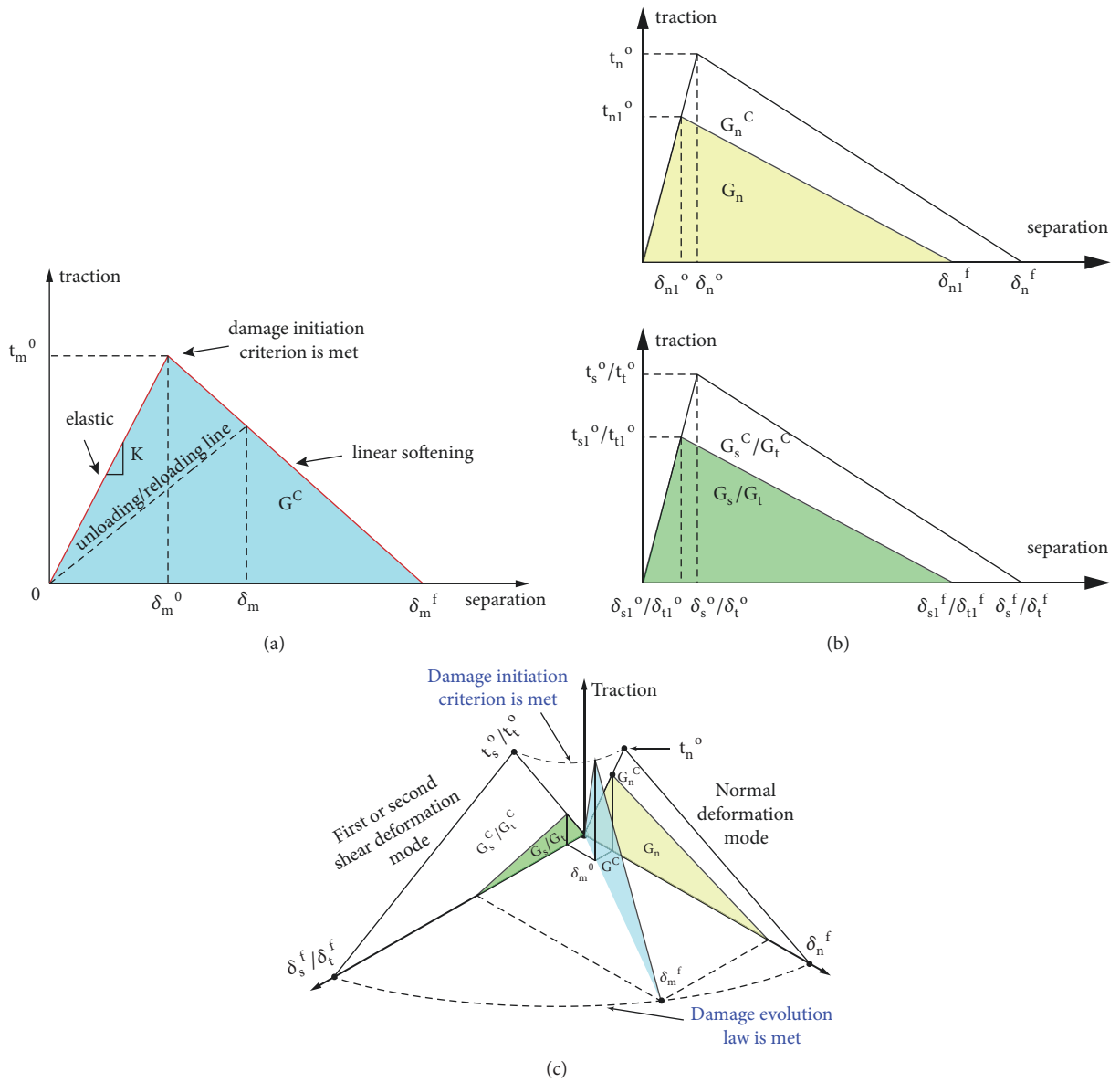

FIGURE 6: Bilinear constitutive traction-separation response of cohesive element: (a) typical bilinear traction-separation model, (b) damage propagation occurring earlier, and (c) mixed-mode bilinear law.

where δ_n, δ_s, and δ_t are the corresponding separation displacements and T_0 is the original thickness of the cohesive element. Thus, the elastic behavior can be described as

$$\boldsymbol{t} = \begin{Bmatrix} t_n \\ t_s \\ t_t \end{Bmatrix} = \begin{bmatrix} K_{nn} & K_{ns} & K_{nt} \\ K_{sn} & K_{ss} & K_{st} \\ K_{tn} & K_{ts} & K_{tt} \end{bmatrix} \begin{Bmatrix} \varepsilon_n \\ \varepsilon_s \\ \varepsilon_t \end{Bmatrix} = \boldsymbol{K\varepsilon}. \quad (14)$$

However, once the damage initiation criterion is met, the interface begins to suffer damage according to the damage evolution law. The following quadratic nominal stress criterion is used to represent the damage initiation criterion:

$$\left\{\frac{\langle t_n \rangle}{t_n^0}\right\}^2 + \left\{\frac{t_s}{t_s^0}\right\}^2 + \left\{\frac{t_t}{t_t^0}\right\}^2 = 1. \quad (15)$$

t_n^0, t_s^0, and t_t^0 are the corresponding peak values of the nominal stress, and $\langle\ \rangle$ is the Macauley bracket.

A scalar damage variable D is used in the linear damage evolution law (like the CDP model for concrete) to denote the overall damage in the interface. After meeting the initiation of damage, D monotonically evolves from 0 to 1 with an increasing load. When the damage variable D reaches 1 at all

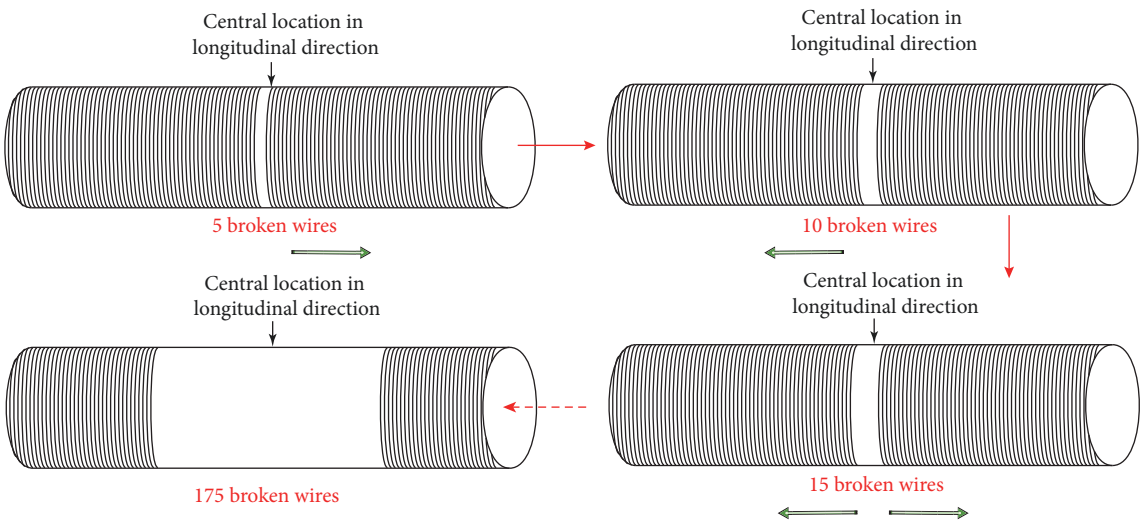

Figure 7: Sequence of wire break in second phase.

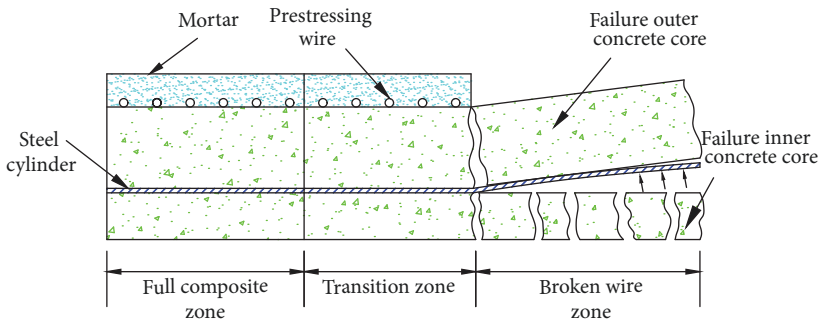

Figure 8: Three distinct zones during wire-break period.

of its material points, the cohesive elements are removed. For linear damage evolution, D is defined as follows:

$$\mathrm{D} = \frac{\delta_m^f \left(\delta_m^{max} - \delta_m^o\right)}{\delta_m^{max} \left(\delta_m^f - \delta_m^o\right)}. \tag{16}$$

δ_m^f is the effective displacement at complete failure, δ_m^o is the effective displacement at the initiation of damage, and δ_m^{max} is the maximum value of the effective displacement attained during the loading history. The stress components at the softening branch that accompany the material stiffness descent can be described as in the following equation:

$$\begin{aligned} t_n &= \begin{cases} (1-D)\,\bar{t}_n, & \bar{t}_n \geq 0 \\ \bar{t}_n, & \text{otherwire (no damage to compressive stiffness)}; \end{cases} \\ t_s &= (1-D)\,\bar{t}_s; \\ t_t &= (1-D)\,\bar{t}_t. \end{aligned} \tag{17}$$

$\bar{t}_n$, $\bar{t}_s$, and $\bar{t}_t$ are the stress components predicted by the elastic traction-separation behavior for the current strains without damage.

Actually, interface will often fail as a mixed mode along three directions in which the relative proportions of the normal and shear deformation are quantified. The damage

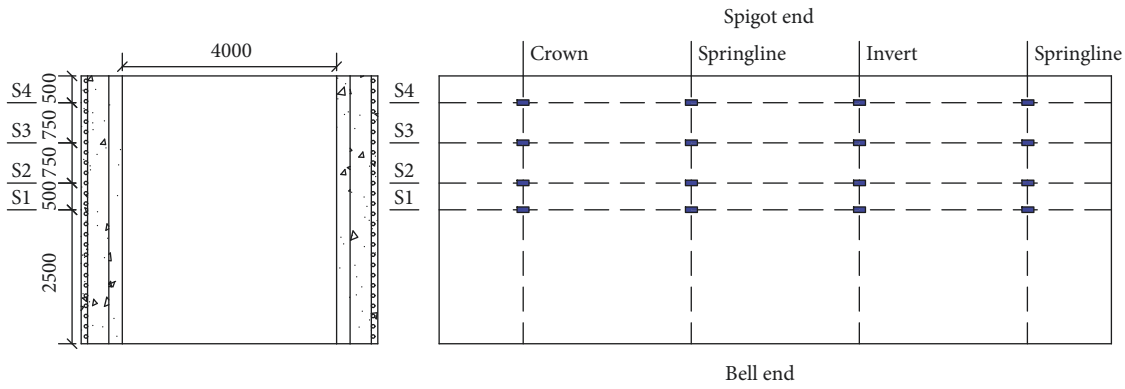

Figure 9: Arrangement of monitoring point on each component.

Table 1: Material properties of PCCP and soil.

Material	Density (kg/m^3)	Young's modulus (MPa)	Poisson's Ratio	Cohesion, c(kPa)	Angle of internal friction, $\varphi(^\circ)$	Dilation, $\psi(^\circ)$
Concrete core	2500	27862	0.2	—	—	—
Mortar coating	2350	25270	0.2	—	—	—
Prestressing wire	7850	193050	0.3	—	—	—
Steel cylinder	7850	206850	0.3	—	—	—
Undisturbed soil zone	2100	250	0.32	65	30	0.1
Bedding soil zone	2000	160	0.34	30	26	0.1
Backfilling soil zone A	2000	180	0.33	35	28	0.1
Foundation of pipe	2000	180	0.33	35	28	0.1
Buffering soil zone	2000	150	0.34	20	25	0.1
Backfilling soil zone B	2000	210	0.33	50	30	0.1

starts propagating even before one of the limit tractions is attained individually, as shown in Figure 6(b). In this figure, t_{n1}^o and δ_{n1}^o represent the peak values of the normal nominal stress and corresponding normal displacement for the mixed mode, and δ_{n1}^f is the failure displacement. The first and second shear directions have similar presentations. Combined with the mixed mode, the damage evolution based on the energy component of the Benzeggagh-Kenane (BK) form is proposed as [33]

$$G_n^C + \left(G_s^C - G_n^C\right)\left\{\frac{G_S}{G_T}\right\}^\eta = G^C;$$
$$G_T = G_n + G_s + G_t; \quad (18)$$
$$G_S = G_s + G_t.$$

G_n, G_s, and G_t are the work done by the tractions and their conjugate relative displacements in the normal, first, and second shear directions, respectively. G^C is the mixed-mode critical fracture. G_n^C and G_s^C refer to the critical fracture energies required to cause failure in the normal and first shear directions. η is a material parameter.

The fracture energy is dissipated as a result of the damage process. It is equal to the area under the traction-separation curve. Figure 6(c) shows a three-dimensional map of the mixed-mode behavior [34].

3.4. Simulated Procedure. The simulated procedure covered two phases: progressively pressurizing to 1.12 MPa in 0.1-MPa intervals, followed by a stepwise wire break under the former steady internal load. The maximum design internal load was 1.12 MPa when considering the working pressure and transient pressure. With an increase in the number of broken wires, the internal load bearing capacity of the pipe decreases continuously. When the number of broken wires is high, the distressed pipe can no longer withstand the original pressure. According to previous experience, the steady pressure should be decreased.

In the second phase, a wire break started at the central location in the longitudinal direction of the pipe. Then, the break extended to the spigot end and bell end alternately with five broken wires at a time. The detailed scenario of the broken wires is shown in Figure 7. When the number of broken wires was from 0 to 60, the internal load was 1.12 MPa; from 65 to 95, 1.00 MPa; from 100 to 135, 0.9 MPa; and from 140 to 175, 0.8 MPa.

Table 2: Material properties of CFRP.

E_{11}	$E_{22} = E_{33}$	$G_{12} = G_{13}$	G_{23}	$\nu_{12} = \nu_{13}$	ν_{23}
75.0 GPa	6.2 GPa	2.3 GPa	2.2 GPa	0.3	0.4

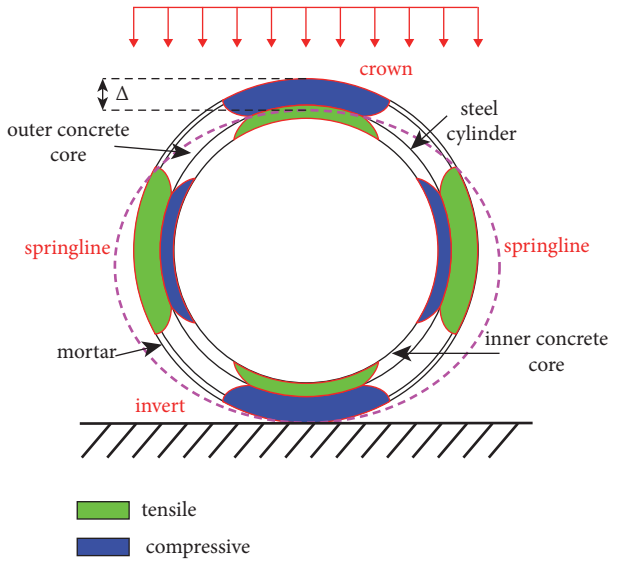

Figure 10: Typical deformation of PCCP under external load (prestressing wire is not present).

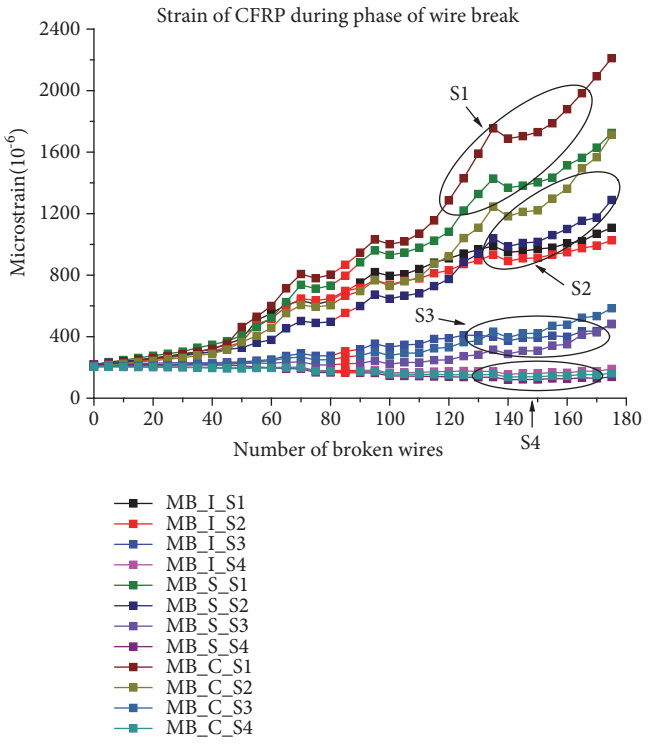

Figure 11: Strain curves of CFRP during phase of wire break.

4. Results and Discussion

During a gradual increase in the number of broken wires, the full composite zone without prestress loss can be converted into a broken wire zone. The pipe was divided into three zones along the longitudinal length to present distinct states during the wire-break phase. As shown in Figure 8, these zones were the full composite zone, the transition zone, and the broken wire zone [35]. The broken wire zone was defined as one in which all wires included in the zone are broken. The transition zone presented the affected zone of the broken wires. The full composite zone presented the undamaged zone, which was far from the broken wire zone.

For each component, strains at the pipe crown, pipe springline, and pipe invert in four sections (S1, S2, S3, and S4 stand for monitoring sections 1, 2, 3, and 4, respectively) were acquired, as shown in Figure 9. The strain curves during the phase of wire break are shown in Figures 11 to 17. The legend XX_Y_ZZ in these figures designates a result with a running model of XX, a hoop location of Y, and a monitoring section of ZZ.

4.1. Phase of Internal Load Increase. Without any broken wires, all components of the pipe remain in the elastic domain. The internal load is mainly withstood by prestressing wires. The strains of the concrete, steel cylinder, wire, and mortar in model A are remarkably close to those in model B. CFRP reaches a peak stress of 11.8 MPa under an internal flow pressure of 1.12 MPa, which is much lower than the ultimate strength. CFRP does not play a role in relieving the deformation of the pipe. Owing to the earth pressure, the deformation at the crown, invert, and springline is different. For CFRP, the inner concrete core, and the steel cylinder, the strains at the springline are greater than those at the crown and invert. By contrast, the strains at the springline are lower than those at the crown and invert for the outer concrete core, wire, and mortar. The reason for this phenomenon is that the external part of the pipe wall at the springline and the interior part of the pipe wall at the crown and invert are tensile, while the opposite parts at these hoop locations are compressive under external loads [36], as shown in Figure 10. The compressive behavior can cause a larger deformation than the tensile behavior.

4.2. Phase of Wire Break

4.2.1. Deformation of CFRP. S1 is always in the broken wire zone. Figure 11 shows the strain of CFRP increasing linearly with the number of broken wires at the beginning of the simulation (0–45). Subsequently, the strain grows rapidly as the number of broken wires increases, which indicates that the concrete core is damaged, and CFRP begins taking a positive effect. The larger the strain, the

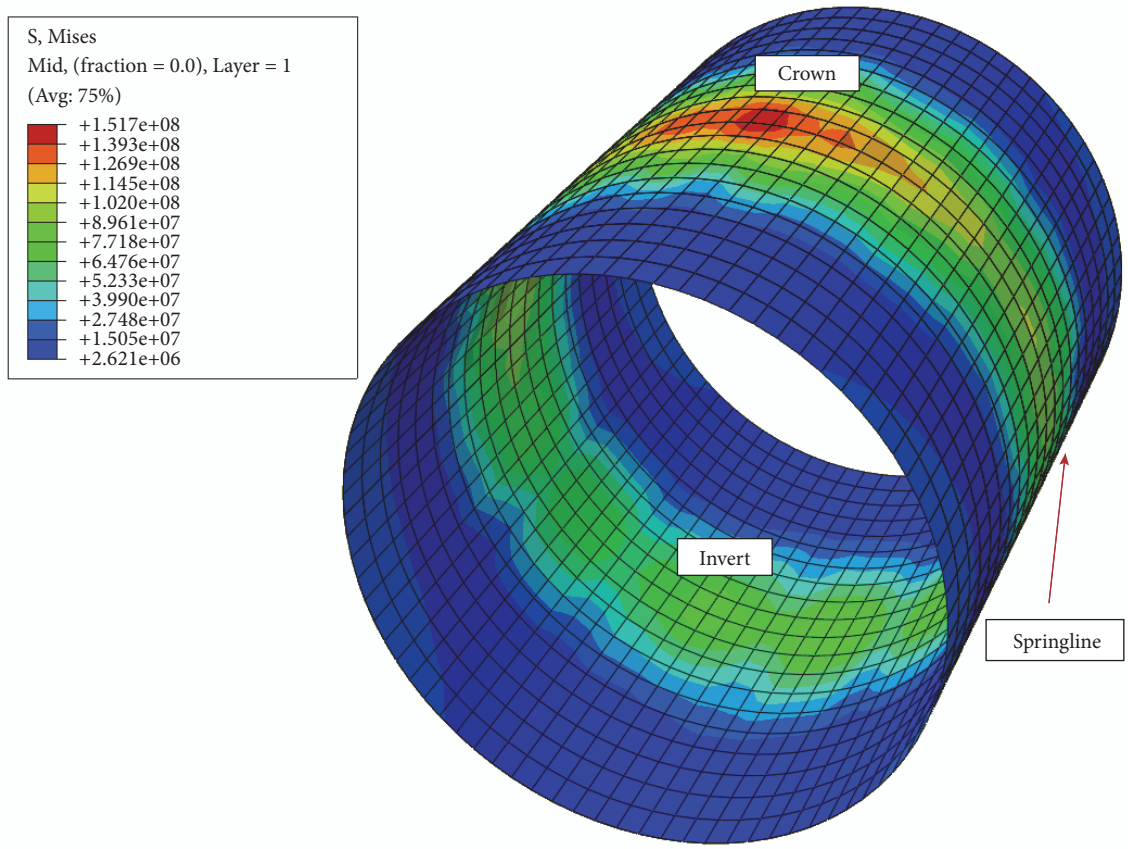

Figure 12: Stress in CFRP at end of phase of wire break.

better the effect of CFRP. Figure 12 shows that the stress of CFRP at the crown for S1 is 151.7 MPa at the end of the phase of wire break, with CFRP as the primary bearing component.

S2 is in the transition zone when the number of broken wires is less than 70 and in the broken wire zone when the number exceeds 75. The impact that the broken wires have on the transition zone decreases successively with an increase in distance. Like the strain of CFRP at S1, the strain at S2 also rises rapidly at a lower rate. The strains at the crown, invert, and springline for S3 stay at a relatively low level, illustrating light damage for S3. S4 is in the full composite zone prior to reaching 160 broken wires. The strain starts growing slightly as the number of broken wires increases further, which indicates that S4 turns into a transition zone. During the entire phase of the wire break, S4 experiences little damage.

In terms of the seriously damaged areas S1 and S2, the strain of CFRP at the crown is greater than that at the invert and springline, stating the crown would fail first as the number of broken wires increases. In other words, the crown is the most seriously damaged part, and CFRP best contributes to its material properties. The three peak values on each curve can be attributed to the decline of the internal flow pressure.

4.2.2. Deformation of Inner Concrete Core. The inner concrete core at S1 experiences compressive plastic damage at 45 broken wires. The higher the number of broken wires, the greater the damage. Since the CDP model does not reflect cracks on concrete directly, 11 times the tensile strain of concrete is taken as the onset of a visual crack [37]. The corresponding hoop strain can be defined as 1524 $\mu\varepsilon$. By comparing the strain in Figures 13(a) and 13(b), the number of broken wires required to cause the onset of a visual crack is acquired, as shown in Table 3. Regarding S1, Table 3 shows that the onset of a visual crack at the crown, springline, and invert for PCCP occurs at 125, 130, and 125 broken wires, respectively. For CFRP-lined PCCP, the number of broken wires is 130, 165, and without a visual crack, respectively.

These results indicate that CFRP causes a stress redistribution and decreases the strain of the inner concrete core. This effect can be seen as protecting the concrete. Regarding the proportion of improvement, the invert shows the strongest increasing trend, followed by the springline and crown. This demonstrates that CFRP has the best rehabilitation effect on the invert, followed by the springline and the crown of the inner concrete core.

Regarding S2, Table 3 indicates that the number of broken wires required to cause onset of visual crack at the crown in model A is 3.13% higher than model B. During the phase of

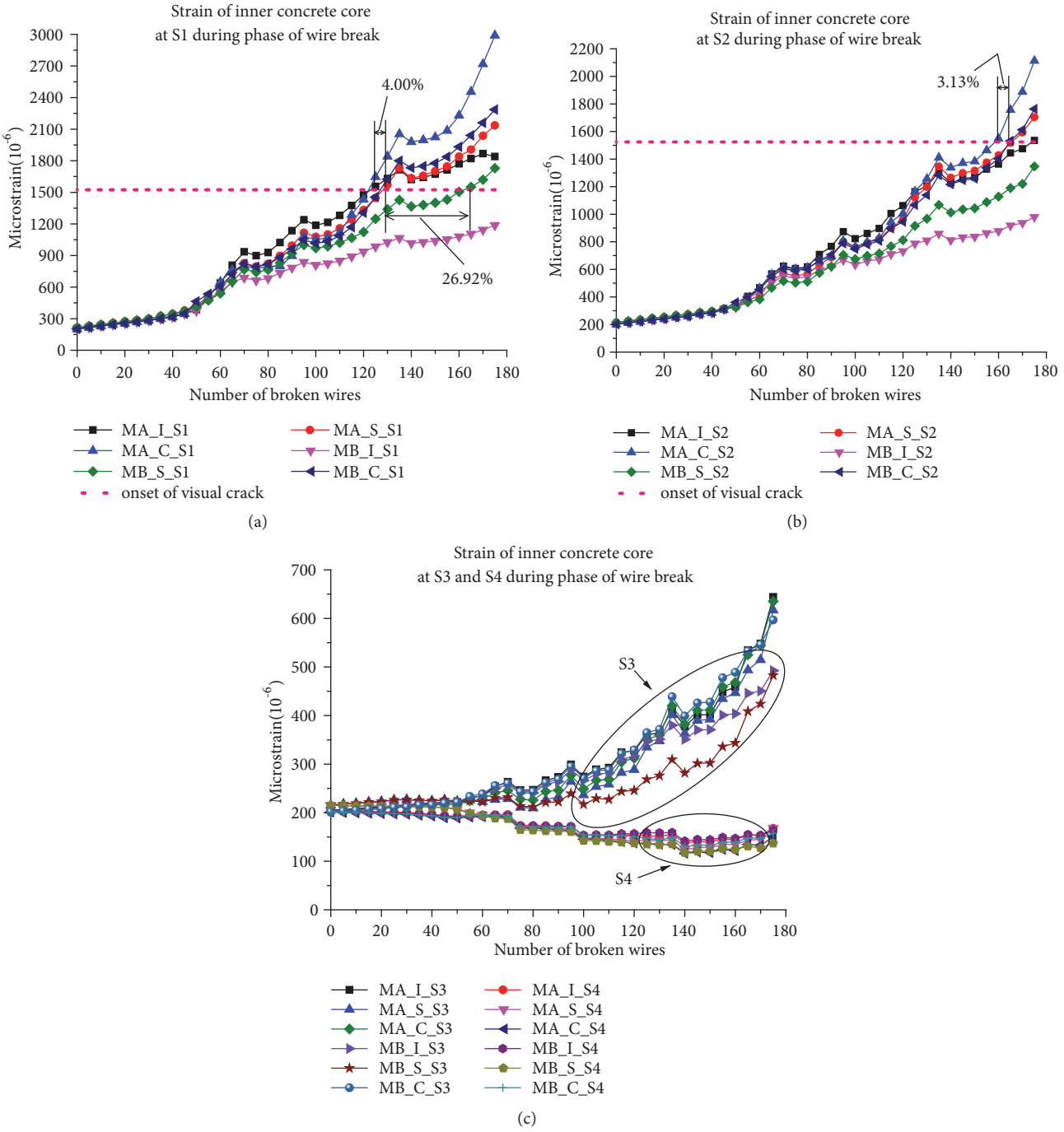

Figure 13: Strain curves of inner concrete core during phase of wire break: (a) strain at S1, (b) strain at S2, and (c) strain at S3 and S4.

Table 3: Number of broken wires required to cause onset of visual crack for inner concrete core.

Component	S1			S2		
	Crown	Springline	Invert	Crown	Springline	Invert
Model A	125	130	125	160	170	175
Model B	130	165	no visual crack	165	no visual crack	no visual crack
Proportion of improvement	4.00%	26.92%	no value	3.13%	no value	no value

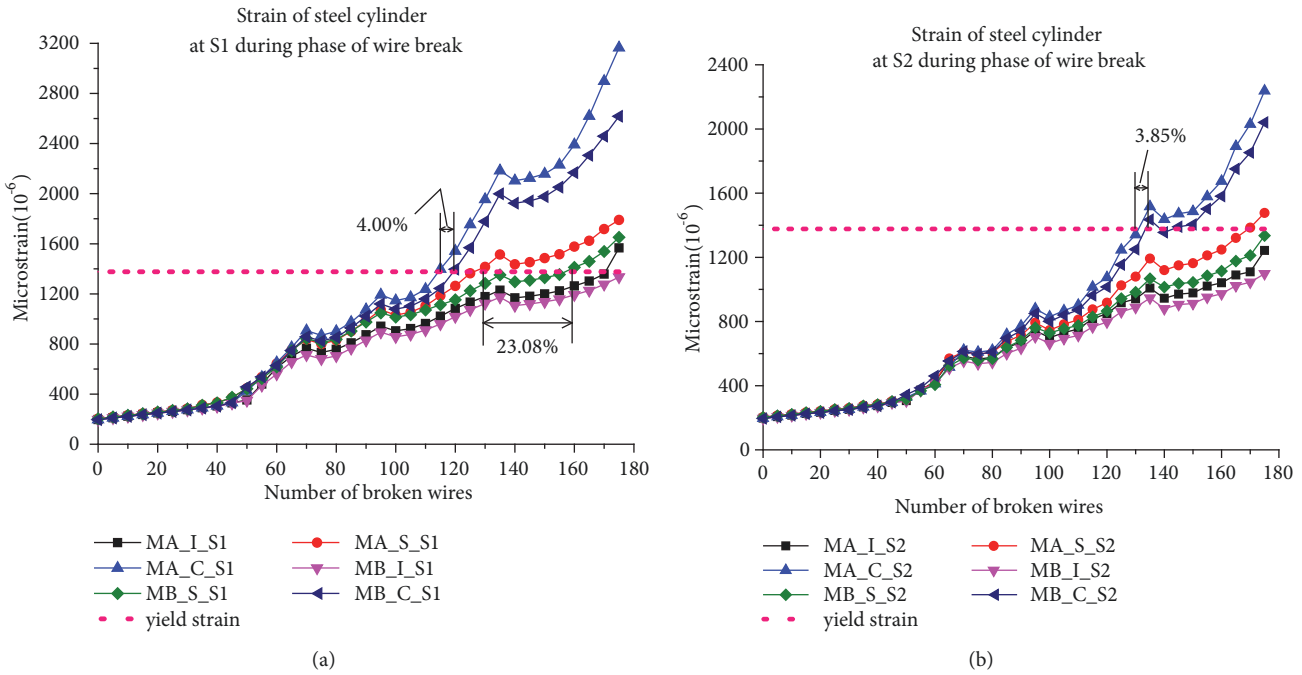

Figure 14: Strain curves of steel cylinder during phase of wire break: (a) strain at S1 and (b) strain at S2.

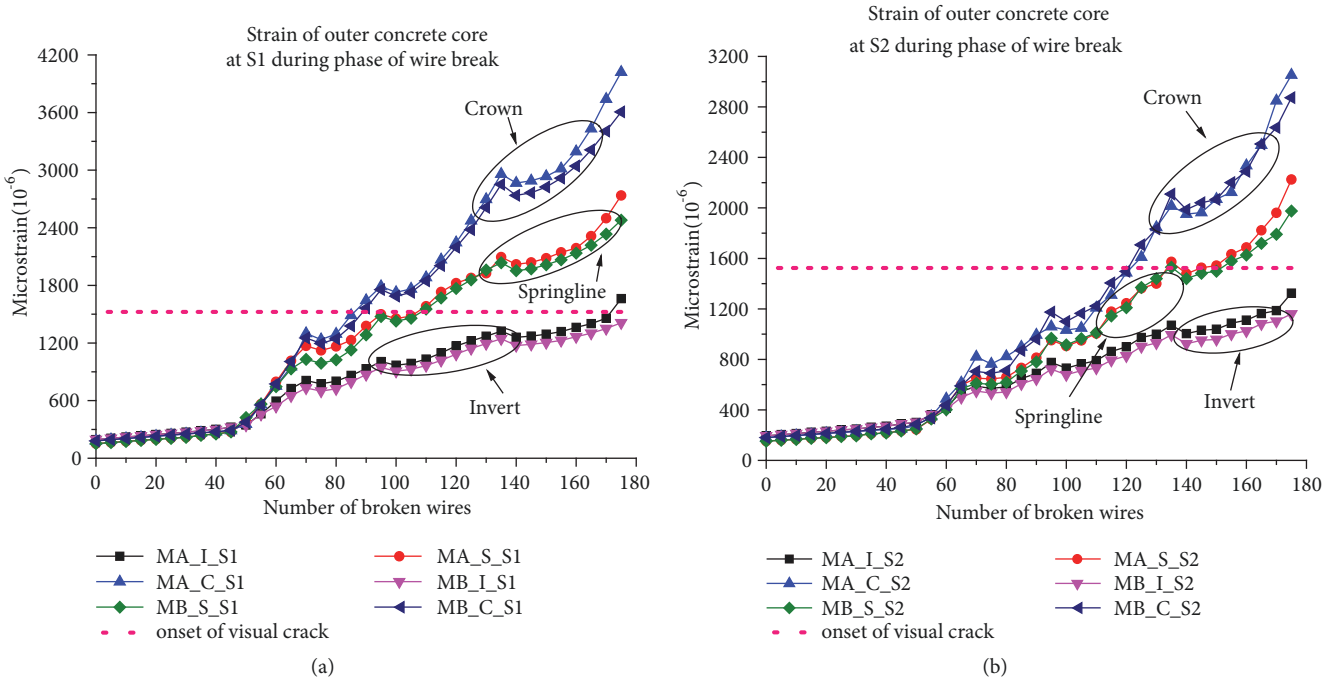

Figure 15: Strain curves of outer concrete core during phase of wire break: (a) strain at S1 and (b) strain at S2.

Table 4: Number of broken wires required to yield the steel cylinder.

Component	S1			S2		
	Crown	Springline	Invert	Crown	Springline	Invert
Model A	115	130	170	130	170	no yield
Model B	120	160	no yield	135	no yield	no yield
Proportion of improvement	4.35%	23.08%	no value	3.85%	no value	no value

Table 5: Area of yielding cylinder and relevant proportions.

Model	Area of yielding cylinder A_y (m^2)	Area of cylinder in broken wire zone A_b (m^2)	Area of entire cylinder A_w (m^2)	A_b/A_w	A_y/A_b	A_y/A_w
Model A	19.75	32.85	65.71	49.99%	60.12%	30.06%
Model B	15.03	32.85	65.71	51.39%	40.51%	20.25%

Table 6: Number of broken wires required to cause onset of visual crack for outer concrete core.

Component	S1			S2		
	Crown	Springline	Invert	Crown	Springline	Invert
Model A	90	110	175	125	135	no visual crack
Model B	90	110	no visual crack	125	135	no visual crack
Proportion of improvement	0.00%	0.00%	no value	0.00%	0.00%	no value

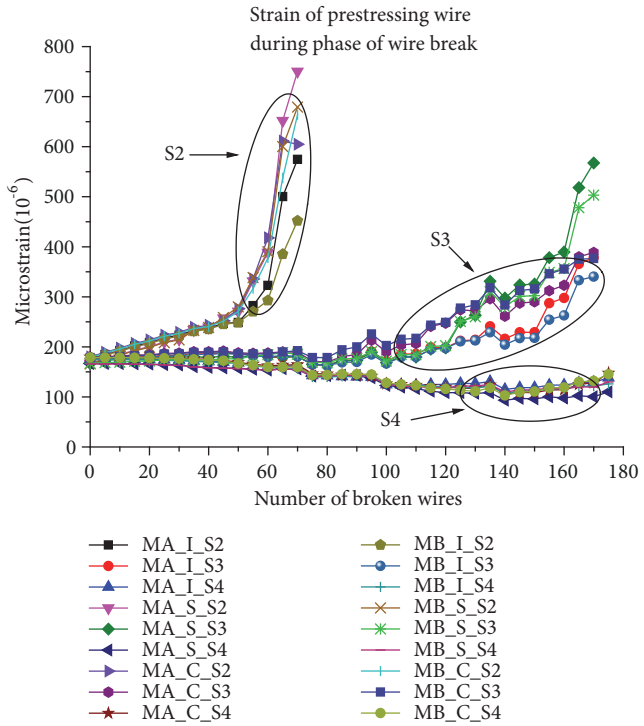

Figure 16: Strain curves of prestressing wire during phase of wire break.

wire break, the springline and invert do not reach the hoop strain of the onset of the visual crack. It is also clear that CFRP relieves the deformation of the springline and invert. Both S3 and S4 are in the full composite zone or transition zone without macrocracks.

4.2.3. Deformation of Steel Cylinder. The strain of the steel cylinder at S1 and S2 shows a rapidly rising rate when the number of broken wires is over 45, which indicates it undertakes part of the internal pressure. Owing to the compressive prestrain provided by prestressing wires, the yield strain of the cylinder is 1377 $\mu\varepsilon$. Table 4 illustrates the number of broken wires required to yield the steel cylinder. Regarding S1, the table shows that yield of the cylinder at the crown, springline, and invert for damaged PCCP occurs at 115, 130, and 170 broken wires, respectively. Meanwhile, the crown and springline in CFRP-lined PCCP show a proportion of improvement of 4.35% and 23.08%, respectively. The cylinder at the invert for S1 in model B never yields. The proportion of improvement at the springline is much higher than that at the crown; this demonstrates that CFRP has a better rehabilitation effect on the springline. Meanwhile, the steel cylinder at the crown yields the earliest, followed by the springline and invert. For S2, the crown and springline require a higher number of broken wires than S1 to yield the cylinder. The steel cylinder at S3 and S4 does not yield.

At the end of the second phase, the yielding areas of the cylinder are counted, as shown in Table 5. This table indicates that the ultimate area of the yielding cylinder in PCCP is as much as 4.72 m^2 larger than that of CFRP-lined PCCP. The proportions for which the area of the yielding cylinder accounts for the area of cylinder in broken wire zone for PCCP and CFRP-lined PCCP are 60.12% and 40.51%, respectively. Obviously, a one-hoop CFRP layer can diminish the yielding range of the cylinder under the same conditions.

4.2.4. Deformation of Outer Concrete Core. The outer concrete core at S1 also exhibits large tensile plastic damage at 45 broken wires. Tensile plastic damage commences at the springline and spreads to the crown and invert with broken wires. Compared to the strain curves in Figure 15, the strains at the same location are very close. Even if the number of broken wires is high, there is only a slight gap between these two curves. The results are also reflected in Table 6. The table shows that the number of broken wires required to crack the outer concrete core visually in model A is the same as that in model B. This is completely different from the inner concrete core. CFRP seems to take no effect. All results indicate that CFRP has little rehabilitation effect on the outer concrete core. The greater the distance from the component to the CFRP, the worse the rehabilitation effect provided by CFRP.

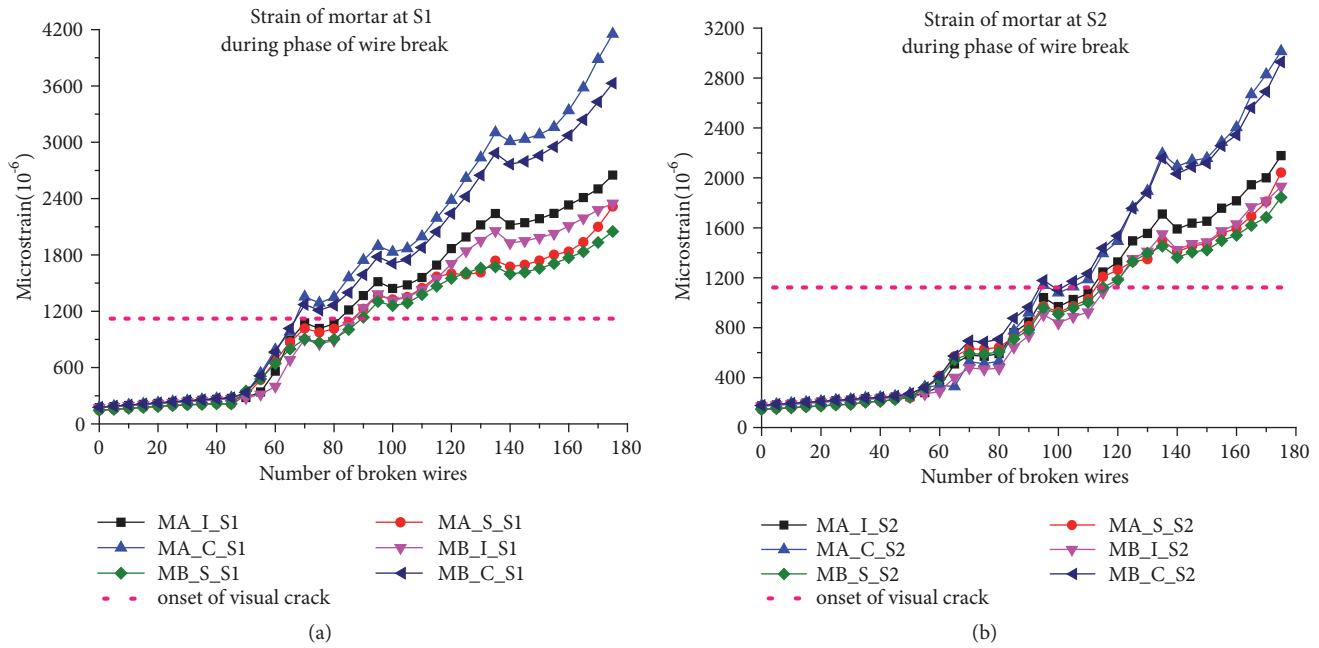

Figure 17: Strain curves of mortar during phase of wire break: (a) strain at S1 and (b) strain at S2.

Table 7: Number of broken wires required to cause onset of visual crack for mortar coating.

Component	S1			S2		
	Crown	Springline	Invert	Crown	Springline	Invert
Model A	70	90	85	95	115	115
Model B	70	90	90	95	115	120
Proportion of improvement	0.00%	0.00%	5.88%	0.00%	0.00%	4.35

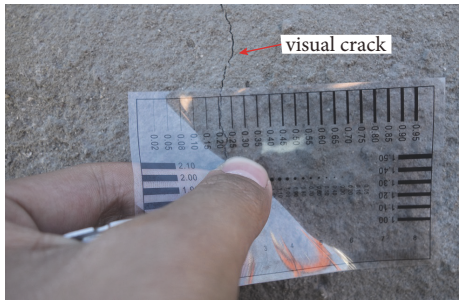

Figure 18: Typical visual crack in mortar.

4.2.5. Deformation of Prestressing Wire. The broken wires are no longer used in the numerical analysis after breakage, which results in no strain in the broken wires, as shown in Figure 16. According to the constitutive relationship in (10) and (11), the actual yield strain of the prestressing wire after wrapping around concrete can be calculated as 1455 $\mu\varepsilon$. Figure 16 illustrates that no prestressing wire yields. The slope of the strain curve at S2 is relatively small when the number of broken wires is less than 50. Subsequently, these curves grow rapidly when the number of broken wires exceeds 50, indicating that the broken wire zone has a more serious influence on the adjacent wire. The regulation of S3 resembles that of S2. In addition, the strain of prestressing wire in model A is remarkably close to that in model B. CFRP does not relieve the deformation of the wire.

4.2.6. Deformation of Mortar Coating. Similar to the concrete core, mortar has a strain that corresponds to the onset of a visual crack. 8 times the tensile strain of mortar is taken, which works out 1133 $\mu\varepsilon$ [37]. The visual crack in the mortar is illustrated in Figure 18. Table 7 shows the number of broken wires required to crack the mortar visually. The results show that S1 and S2 in model A and model B have the same cracking index at the crown and springline and an offset of only five broken wires at the invert. This phenomenon can be seen as there being little distinction between PCCP and CFRP-lined PCCP.

Before onset of a visual crack, CFRP takes little effect on the mortar. As shown in Figures 17(a) and 17(b), the gaps in the strain curves between PCCP and CFRP-lined PCCP at the same monitoring point increase as the number of broken wire wraps increases after the onset of a visual crack. This indicates that CFRP starts working to relieve the deformation of the mortar. The higher the number of broken wires, the more serious the damage level in the pipe, and the better the CFRP effect. Moreover, CFRP only has an obvious effect on

the distressed PCCP, which is verified on the concrete core and steel cylinder.

5. Conclusions

In this paper, two contrasting three-dimensional FE models were established to evaluate the rehabilitation effect of CFRP-lined PCCP during a phase of internal load increase and a phase of wire break considering combined loads. A conceptual zone was introduced to analyze the structural performance of all components in different zones. The state of the pipe was investigated by examining two critical indicators: visual cracking of the concrete and mortar, and the yielding of the steel cylinder. The following conclusions were drawn from this study:

(1) In terms of the PCCP during the phase of wire break, components at the crown fail first, followed by the springline and invert.

(2) CFRP has a distinct rehabilitation effect on various components. The farther the distance from the component to CFRP, the worse the rehabilitation effect provided by CFRP. Namely, CFRP clearly reduces the development of cracking in the inner concrete core and relieves the yield of the steel cylinder while having little effect on the outer concrete, prestressing wire, or mortar.

(3) For the same component, CFRP also has a different rehabilitation effect at different locations. The deformation relieved by CFRP is the largest at the invert, then at the springline, and was smallest at the crown. Meanwhile, a one-hoop CFRP layer diminishes the area of a yielding steel cylinder of 4.72 m^2.

(4) CFRP only has a clear effect on distressed PCCP. Moreover, CFRP works more effectively with an increase in the number of broken wires. For a full composite zone and transition zone, CFRP has no effect.

Data Availability

The figures and tables data used to support the findings of this study are included within the article. In addition, the finite element models are available from the corresponding author upon request.

Conflicts of Interest

The authors declare that there are no conflicts of interest regarding the publication of this paper.

Acknowledgments

This work was supported by the Beijing Municipal Science and Technology Commission (no. Z141100006014058) and the Science and Technology Service network program (STS) project (no. KFJ-STS-ZDTP-037) of the Chinese Academy of Sciences.

References

[1] A. Selvakumar, R. M. Clark, and M. Sivaganesan, "Costs for water supply distribution system rehabilitation," *Journal of Water Resources Planning and Management*, vol. 128, no. 4, pp. 303–306, 2002.

[2] B. Simpson, N. A. Hoult, and I. D. Moore, "Rehabilitated reinforced concrete culvert performance under surface loading," *Tunnelling and Underground Space Technology*, vol. 69, pp. 52–63, 2017.

[3] S. Rahman, G. Smith, R. Mielke, and B. Keil, "Rehabilitation of large diameter PCCP: relining and sliplining with steel pipe," in *Proceeding of the Pipelines 2012: Innovations in Design, Construction, Operations, and Maintenance, Doing More with Less*, pp. 494–504, Miami Beach, FL, USA, 2012.

[4] G. R. Boyd, N. K. Tarbert, R. J. Oliphant, G. J. Kirmeyer, B. M. Murphy, and R. F. Serpente, "Lead pipe rehabilitation and replacement techniques for drinking water service: Review of available and emerging technologies," *Tunnelling and Underground Space Technology*, vol. 15, no. 1, pp. 13–24, 2000.

[5] D. C. Lee and V. M. Karbhari, "Rehabilitation of large diameter prestressed cylinder concrete pipe (PCCP) with FRP composites - Experimental investigation," *Advances in Structural Engineering*, vol. 8, no. 1, pp. 31–44, 2005.

[6] M. S. Zarghamee and M. Engindeniz, "Watertightness of CFRP Liners for Distressed Pipes," in *Proceedings of the Pipelines 2015 Conference: Recent Advances in Underground Pipeline Engineering and Construction*, pp. 1533–1543, Baltimore, MD, USA, August 2015.

[7] Q. Gong, H. Zhu, Z. G. Yan, B. Q. Huang, Y. Zhang, and D. Y. Dong, "Fracture and delamination assessment of prestressed composite concrete for use with pipe jacking method," *Mathematical Problems in Engineering*, vol. 2015, Article ID 579869, 11 pages, 2015.

[8] Y. Lee, M. Q. Feng, and E.-T. Lee, "Deflection of buried prestressed concrete cylinder pipe with soil-pipe interaction," *KSCE Journal of Civil Engineering*, vol. 18, no. 7, pp. 2191–2195, 2014.

[9] H. Xiong, P. Li, and Q. Li, "FE model for simulating wire-wrapping during prestressing of an embedded prestressed concrete cylinder pipe," *Simulation Modelling Practice and Theory*, vol. 18, no. 5, pp. 624–636, 2010.

[10] M. Hajali, A. Alavinasab, and C. Abi Shdid, "Structural performance of buried prestressed concrete cylinder pipes with harnessed joints interaction using numerical modeling," *Tunnelling and Underground Space Technology*, vol. 51, pp. 11–19, 2016.

[11] X. Z. Lu, L. P. Ye, J. G. Teng, and J. J. Jiang, "Meso-scale finite element model for FRP sheets/plates bonded to concrete," *Engineering Structures*, vol. 27, no. 4, pp. 564–575, 2005.

[12] X. Z. Lu, J. G. Teng, L. P. Ye, and J. J. Jiang, "Bond–slip models for FRP sheets/plates bonded to concrete," *Engineering Structures*, vol. 27, no. 6, pp. 920–937, 2005.

[13] H. Zhang, S. T. Smith, R. J. Gravina, and Z. Wang, "Modelling of FRP-concrete bonded interfaces containing FRP anchors," *Construction and Building Materials*, vol. 139, pp. 394–402, 2017.

[14] W. Sun, X. Peng, and Y. Yu, "Development of a simplified bond model used for simulating FRP strips bonded to concrete," *Composite Structures*, vol. 171, pp. 462–472, 2017.

[15] K. Narmashiri, M. Jumaat, and N. Sulong, "Strengthening of steel I-beams using CFRP strips: An investigation on CFRP bond length," *Advances in Structural Engineering*, vol. 15, no. 12, pp. 2191–2204, 2012.

[16] M. S. Zarghamee, M. Engindeniz, and N. Y. Wang, "CFRP renewal of prestressed concrete cylinder pipe," WRF Web Report 4352, Water Research Foundation, 2013.

[17] Y. Lee and E.-T. Lee, "Analysis of prestressed concrete cylinder pipes with fiber reinforced polymer," *KSCE Journal of Civil Engineering*, vol. 19, no. 3, pp. 682–688, 2015.

[18] M. S. Zarghamee, M. Engindeniz, O. O. Erbay, and R. P. Ojdrovic, "Repair of concrete pressure pipes with CFRP composites," in *Proceedings of the Structures Congress*, pp. 1874–1884, Orlando, FL, USA, May 2010.

[19] N. Wang and M. S. Zarghamee, "LRFD approach to CFRP renewal of prestressed concrete cylinder pipes," in *Proceedings of the Pipelines 2012: Innovations in Design, Construction, Operations, and Maintenance, Doing More with Less*, pp. 481–493, Miami Beach, FL, USA, August 2012.

[20] M. S. Zarghamee and M. Engindeniz, "CFRP Renewal of Prestressed Concrete Cylinder Pipe: part 2," WRF Web Report 4510, Water Research Foundation, 2014.

[21] H. R. Lotfi, R. G. Oesterle, and J. Roller, "Reliability assessment of distressed prestressed concrete cylinder pipe," in *Proceedings of the Pipelines 2005: Optimizing Pipeline Design, Operations, and Maintenance in Today's Economy*, pp. 838–852, Houston, TX, USA, 2005.

[22] M. G. Katona, "Influence of soil models on structural performance of buried culverts," *International Journal of Geomechanics*, vol. 17, no. 1, 2017.

[23] S. Alzabeebee, D. N. Chapman, and A. Faramarzi, "Numerical investigation of the bedding factor of concrete pipes under deep soil fill," in *Proceedings of the 2nd World Congress on Civil, Structural, and Environmental Engineering (CSEE '17)*, pp. 1–8, Barcelona, Spain, April 2017.

[24] ABAQUS, *User's Manual 6.13*, Dassault Systemes Simulia, Providence, RI, USA, 2013.

[25] J. Lubliner, J. Oliver, S. Oller, and E. Oñate, "A plastic-damage model for concrete," *International Journal of Solids and Structures*, vol. 25, no. 3, pp. 299–326, 1989.

[26] J. Lee and G. L. Fenves, "Plastic-damage model for cyclic loading of concrete structures," *Journal of Engineering Mechanics*, vol. 124, no. 8, pp. 892–900, 1998.

[27] ANSI/AWWA C304-2007, *Design of Prestressed Concrete Cylinder Pipe*, American Water Works Association, Denver, CO, USA, 2007.

[28] GB 50010-2010, *Code for Design of Concrete Structures*, Architecture and Building Press, Beijing, China, 2010.

[29] SL 702-2015, *Technical Specifications of Prestressed Concrete Cylinder Pipe*, China Water and Power Press, Beijing, China, 2015.

[30] T. Xu, Z. J. He, C. A. Tang, W. C. Zhu, and P. G. Ranjith, "Finite element analysis of width effect in interface debonding of FRP plate bonded to concrete," *Finite Elements in Analysis and Design*, vol. 93, pp. 30–41, 2015.

[31] X. Z. Lu, J. J. Jiang, J. G. Teng, and L. P. Ye, "Finite element simulation of debonding in FRP-to-concrete bonded joints," *Construction and Building Materials*, vol. 20, no. 6, pp. 412–424, 2006.

[32] W. Sun, X. Peng, H. Liu, and H. Qi, "Numerical studies on the entire debonding propagation process of FRP strips externally bonded to the concrete substrate," *Construction and Building Materials*, vol. 149, pp. 218–235, 2017.

[33] M. L. Benzeggagh and M. Kenane, "Measurement of mixed-mode delamination fracture toughness of unidirectional glass/epoxy composites with mixed-mode bending apparatus," *Composites Science and Technology*, vol. 56, no. 4, pp. 439–449, 1996.

[34] P. P. Camanho and C. G. Davila, "Mixed-Mode decohesion finite elements for the simulation of delamination in composite materials," NASA/TM-2002–211737, 2002.

[35] O. O. Erbay, M. S. Zarghamee, and R. P. Ojdrovic, "Failure risk analysis of lined cylinder pipes with broken wires and corroded cylinder," in *Proceedings of the Pipelines 2007: Advances and Experiences with Trenchless Pipeline Projects*, pp. 1–10, Boston, MA, USA, July 2007.

[36] Y. Zhang, Z.-G. Yan, H.-H. Zhu, and J. W. Ju, "Experimental study on the structural behaviors of jacking prestressed concrete cylinder pipe," *Tunnelling and Underground Space Technology*, vol. 73, pp. 60–70, 2018.

[37] M. S. Zarghamee and K.-L. Fok, "Analysis of prestressed concrete pipe under combined loads," *Journal of Structural Engineering*, vol. 116, no. 7, pp. 2022–2039, 1990.